Journal of Heat and Mass Transfer Research

Journal homepage: https://jhmtr.semnan.ac.ir

Semnan University

ISSN:2383-3068

Research Article

Enhanced Heat Transfer in a Vertical Heated Channel by Incorporation of Inclined Plates

Nabila Trad, Rabah Henniche*, Abdelkader Korichi

Faculty of Technology, Laboratory of Mechanics, Physics and Mathematical Modeling (LMP2M), University of Medea, 26000, Medea, Algeria

ARTICLE INFO

Article history:

Received: 2025-03-27

Revised: 2025-06-15

Accepted: 2025-07-12

Keywords:

Mixed convection;

Heat transfer enhancement;

Unsteady flow;

Plates;

Channel.

ABSTRACT

This study aims to investigate fluid flow and heat transfer behaviors under laminar mixed convective conditions in a vertical heated channel with plates attached to the heated wall in order to enhance the cooling channel. Simulations were conducted using the finite volume method through the OpenFoam © open-source code. The analysis focused on three key physical parameters: Reynolds number varying from 200 to 1400, Grashof number set at 10^5 and 2×10^5, and three plate tilt angles (γ = 30°, 60°, and 90°), with a fixed plate height of h_p = 0.3 and a constant plate spacing of D = 1. The objective was to assess their effects on thermal and flow behaviors in both steady-state and self-sustained oscillatory flow. The results were presented as dimensionless isotherm contours and streamlines, accompanied by the Nusselt number and friction factor ratios. Findings indicate that both the friction factor and Nusselt number ratios increase as Reynolds number and plate tilt angles increase, while they decrease as the Grashof number increases. The flow translates to a self-sustained oscillatory state at moderate Reynolds numbers (below 1000 for γ = 60° and 90°, below 1200 for γ = 30°). Moreover, as the flow bifurcates to an unsteady state, the Nusselt number significantly increases and can reach up to 18%, 54% and 60% for γ = 30°, 60° and 90°, respectively, compared to the channel without plates. The unsteady flow pattern contributes to enhancing the heat transfer by disturbing the near-wall region. Notably, the plate tilt angle of γ = 30° achieves an optimal balance between enhancing heat transfer efficiency and reducing flow resistance. From these results, it can be concluded that this study is useful for the design efficiency of electronic cooling systems and heat exchangers that can provide maximum heat transfer with minimum flow resistance.

1. Introduction

Heat transfer enhancement refers to the methods and techniques used to increase the rate of heat exchange between a fluid and a solid surface or between two fluids. These methods are crucial for conserving energy and optimizing the use of energy resources. Enhancing heat transfer is essential for achieving high efficiency while reducing the size, weight, and cost of systems. Additionally, the heat transfer process has been widely applied in thermal systems applications such as compact heat exchangers, solar collector systems, chemical reactors, air conditioning, power generation, and electronic cooling. From previous work, much effort has focused extensively on developing economical methods to improve the efficiency of thermal systems. Different approaches, including active, passive, and compound methods, are used to improve heat transfer. Active methods require external energy input to improve the process, whereas passive methods do not need any additional energy to improve the thermal

* **Corresponding author.**

E-mail address:rabahh200@yahoo.fr

Cite this article as:

Trad, N., Henniche, R., and Korichi, A., 2026. Enhanced Heat Transfer in a Vertical Heated Channel by Incorporation of Inclined Plates. *Journal of Heat and Mass Transfer Research*, 13(1), pp. 1-17.

https://doi.org/10.22075/JHMTR.2025.37223.1700

efficiency of the systems. Passive and active techniques can also be combined together, called compound techniques, to achieve a higher gain than using either approach independently. Passive methods require modifications to the geometry or surface of the flow channel in order to augment thermal performance. Plates, ribs, fins, baffles, and rough surfaces are used to promote fluid mixing and improve heat transfer rates. Active methods are more complex in design and application than passive methods due to the necessity for external energy to adjust fluid flow and increase thermal efficiency. The difficulty of supplying external energy in various applications limits the use of active methods in scientific fields. Passive methods, which perturb the near-wall region using vortex generators, and active methods that employ moving objects or modulated flows have been cited by [1, 2, 3, 4]. Various numerical and experimental studies have been performed to analyze how the different parameters can enhance the efficiency of thermal systems while simultaneously reducing their size and energy consumption.

Garimella and Eibeck [5] conducted experimental research on the effect of vortex generator prostration on heat transfer from an array of discrete heat sources. They reported a maximum heat transfer improvement of approximately 40%. Roberts [6] carried out both numerical and experimental investigations of fluid flow and heat transfer in a channel with baffles arranged in series and periodically along both walls. The results demonstrate that at low Reynolds numbers, the flow remains steady and symmetrical, with recirculation bubbles forming after each baffle. However, as the Reynolds number approaches a critical value of around 100, the flow becomes asymmetric and unsteady. The two-dimensional numerical results for laminar flow are closely aligned with both steady and unsteady experimental results. In the turbulent regime, however, the experimental results reveal a secondary transition to three-dimensional behavior. In another study conducted by Wang et al. [7], it was observed that in the inline configuration, the flow becomes unsteady at a critical Reynolds number of approximately 110. However, for the staggered configuration, this critical value increases to 200. Their results indicate a significant increase in the heat transfer rate as the flow translates to an unsteady state. However, this increase is consistently accompanied by a higher pressure drop. Yuan et al. [8] conducted an experimental investigation into heat transfer and flow dynamics in a channel with periodic rectangular fins aligned with the main flow direction. Their findings highlight an increase in heat transfer compared to the results from a similar channel without baffles. Fu and Tong [9] carried out a numerical simulation to examine the effect of an oscillating cylinder on the heat transfer of heated blocks in channel flow. The results demonstrate a significant improvement in heat transfer when the oscillation frequency of the cylinder falls within the lock-in region. Mousavi and Hooman [10] confirmed that increasing the Reynolds and Prandtl numbers results in a higher Nusselt number along the isothermal channel walls in a horizontal configuration with alternating baffles. Ko and Anand [11] conducted experimental measurements to investigate fluid flow and heat transfer in a heated rectangular channel with porous baffles installed on both walls. Their results showed that the use of porous baffles increased the heat transfer rate by over 300% compared to a channel without baffles. However, this increase in heat transfer rate was accompanied by a significant increase in flow energy. Guzmán and Del Valle [12] conducted a numerical study to investigate the transition scenario and heat transfer characteristics in grooved channels as the flow regime progresses from laminar to transitional. They found that the average heat transfer rate remains largely constant during the laminar steady regime, but it consistently increases during the transitional regime. The heat transfer enhancement is greater in a quasi-periodic flow regime than in a periodic one. This enhancement is twice as significant in the periodic flow regime and can be two and a half times higher in the quasi-periodic regime compared to a smooth channel. Fu et al. [13] carried out an experimental study to determine the heat transfer data in a rectangular channel with an aspect ratio (AR = 2:1) with discrete and V-shaped baffles. Their findings revealed that both V-shaped baffles and discrete V-shaped baffles exhibited greater heat transfer improvement compared to 45° angled baffles and discrete 45° angled baffles for both rotating and non-rotating cases. In another study, Liu et al. [14] discovered that as the rib pitch-to-height ratio of the channel decreases, the Nusselt number ratios tend to increase. Moreover, when the rib pitch-to-height ratio decreases to 3, there is a decrease in the friction factor. Wright and Gohardani [15] utilized V-shaped ribs in rectangular and trapezoidal cooling passages with coolant ejection. Their conclusion was that the entrance condition is borderline when both V-shaped ribs and coolant extraction are taken into account in the trapezoidal channel. The use of porous and solid baffles attached to both walls in an offset manner in a rectangular channel for the laminar steady-state condition has been carried out by Santos and Lemos [16] and Zhang

et al. [17]. Their results confirmed that the baffles cause flow separation/attachment, which affects the local heat transfer efficiency. Furthermore, both studies concluded that similar rates of heat transfer enhancement can be achieved with both solid and porous baffles. Nonetheless, the use of solid baffles results in an increase in the friction factor.

Promvonge et al. [18] conducted numerical investigations on the periodic laminar flow and heat transfer properties within a square channel featuring 30° inline angled baffles attached to the opposite channel walls. Their results revealed that the angled baffles generated streamwise main vortex flows, which facilitated impingement flows on the channel walls, thereby significantly enhancing the heat transfer rate. Promvonge et al. [19] in another study found that the presence of 45° angled baffles causes a remarkable improvement in the heat transfer rate by 150 to 850% over the blockage ratio range of 0.05 to 0.3. However, in the case of 45° angled baffles, the heat transfer improvement is approximately 100 to 200% higher than that of 90° baffles, while also providing a reduction in the friction factor of approximately 10 to 150%. Peng et al. [20] conducted experimental and numerical investigations on the heat transfer improvement in a channel with different types of baffles. Their findings indicate that the use of 45° V-shaped baffles provides a higher improvement in the heat transfer rate. Lopez et al. [21] numerically analyzed the dynamic and thermal effects by varying the location of regular baffles in a 3D channel. Their results revealed that the three-dimensional influence on the friction factor becomes increasingly significant at higher Reynolds number values. Guo and Anand [22] studied the three-dimensional convective heat transfer flow in a channel with a single baffle placed near the inlet region. Their overall observations indicated that as the Reynolds number and the dimension of the baffle increased, both the separation length upstream of the baffle and the length of the recirculation zone downstream of the baffle also increased. Tsay et al. [23] examined the heat transfer improvement due to the insertion of a transverse baffle in a channel with a backward-facing step. The effect of baffle size, thickness, and spacing of the baffle regarding the backward-facing step on the flow characteristics is investigated for Reynolds number values in the range of 100 to 500. Their findings proved that the placement of a baffle in the channel can increase the global Nusselt number by up to 190%. Moreover, they illustrated that the heat transfer rate and fluid flow patterns are greatly dependent on the baffle position. Tehrani and Abadi [24] presented a study on the dynamic and thermal behavior of flow in a duct equipped with a series of baffles. Their results revealed that baffle-type obstacles are rather ineffective for large values of blockage ratio.

The effect of buoyant assisted flow on the heat exchange and fluid dynamics structure in an asymmetrically heated channel containing a series of identical conductive equidistant baffles has been numerically analyzed by Cheng et al. [25] and Cheng and Yang [26]. Their results unveiled the appearance of a sequence of vortices near the cold wall when the wall is heated sufficiently, and an opposite pressure gradient can be developed in the downstream channel. Moreover, they observed that heat transfer is improved as baffle heights or the space between the baffles is increased. On the other hand, Fung and Lazaridis [27] found that, in addition to the flow recirculation that occurs downstream of each fin/baffle, the buoyant flow effect induces a vortex near the cold wall that tends to reduce heat transfer. The primary vortex behind the fin on the hot wall expands as the Reynolds number increases, while the secondary vortex near the cold wall is suppressed. This phenomenon reduces heat transfer at the hot wall and changes the evolution of temperature profiles. The degradation in heat transfer became increasingly noticeable as the Prandtl number increased. In addition, the geometric parameters affect both heat transfer and the friction factor at the channel's walls. The effect of a baffle installed on the unheated wall of a vertical channel on mixed convection under opposing effects and pulsating flow has been examined by Chang and Shiau [28]. The influence of pulsation frequency, Prandtl number, and baffle position is examined across various Richardson number (Ri) values. The results highlight that the use of a baffle and pulsating flow leads to improved heat transfer. Moreover, the global Nusselt number shows a notable increase for large values of Reynolds number, pulsation amplitude, and Prandtl number. Fu et al. [29] conducted a numerical examination of heat transfer enhancement in a three-dimensional vertical channel experiencing mixed convection flow by introducing a moving thin block. They observed that a higher Reynolds number leads to an improved heat transfer rate when the Gr/Re^2 ratio is low. However, when the buoyancy force becomes substantial, the heat transfer rate diminishes. A numerical study of upward mixed convection in a channel with a sequence of baffles attached to the heated wall has been analyzed by Nemitallah and Zohir [30]. Their results proved that the radiation of heat transfer becomes significant and cannot be neglected if

the wall heating is strong enough. Furthermore, a positive pressure gradient is developed along the channel axis and triggers the formation of recirculation zones near the cold wall beyond a critical value of Gr/Re^2. The size of these recirculation zones increases with increasing heating intensity.

Chang [31] presented a numerical study on laminar mixed convective flow in a three-dimensional square channel with the presence of one baffle attached to the unheated wall. He observed that under high buoyancy effect conditions, a recirculating region forms near both the top wall and the hot surface. However, the restricted flow zone induced by the baffle can accelerate the flow, resulting in an enhanced heat transfer rate. The author also noted that the enhancement of heat transfer is contingent upon both the position of the baffle and the presence of recirculation zones. Henniche and Korichi [32] conducted numerical estimations of laminar heat transfer enhancement in a vertical baffled heated channel. Their analysis revealed that this baffled channel leads to approximately 2.8 times heat transfer augmentation when the non-dimensional baffle height is 0.25. However, they noted that this specific non-dimensional baffle height provides a favorable balance between heat transfer enhancement and pumping power. Thermal exchange, pressure drops, and thermohydraulic behavior inside an airflow channel with many V-type baffles have been studied experimentally by Kumar et al. [33]. Their outcomes effectively showed that the optimal improvement of overall thermal efficiency has been obtained when the discrete distance is 0.67, the blockage ratio is 0.5, the gap width is 1, the baffle spacing is 10, and the attack angle is 60°. The influence of baffles positioned in various configurations with distinct ratios of perforation on thermal exchange, flow friction, and thermal efficiency through a rectangular channel within Reynolds numbers in the range of 12000 to 32000 has been numerically and experimentally reported by El Habet et al. [34]. Outcomes proved that the different configurations of baffles lead to an increase in the heat transfer rate by 15 to 310% compared to the same no-baffles channel. However, the case of staggered arrangement has less flow friction and significant thermal efficiency than the case of inline arrangement within the full interval of Reynolds numbers. Kurian et al. [35] examined an experimental investigation on flow behavior in jet impingement systems employing segmented and perforated baffle arrangements. Their results have shown that the highest rate of heat transfer is obtained for the segmented structure compared to that of the perforated structure. However, the segmented configuration has given a high pressure drop in spite of the augmentation in heat transfer. Also, the louvered shape decreased pressure drop and heat transfer comparatively with the segmented shape. They concluded that, as the jet to baffle distance decreases, thermohydraulic performance increases considerably. Recently, Henniche and Korichi [36] conducted a review of heat transfer improvement in mixed and forced convection in baffled channels. Their findings highlighted that the inclusion of baffles significantly improved the extent of heat transfer. However, this extent was influenced by the specific shape of the baffles.

The analysis of the above literature indicates that most studies focus on pure forced convection, while only a few address mixed convection, which treats the steady-state phenomena or employs a steady-state algorithm that eliminates all fluctuations (see [10, 16, 25]). The presence of plates, along with buoyancy forces, creates significant interactions that push the flow into the unsteady regime. Additionally, the unsteady behavior and the interaction between inertial and buoyancy forces create a challenging simulation task that demands substantial hardware resources and time. Thus, this study fits within this domain and attempts to improve the understanding of the unsteady phenomenon by closely approximating the reality of the problem. However, the unsteady, laminar, incompressible, and mixed convective flow of a Newtonian fluid in a vertical channel with inclined plates, which occurs in heat exchangers, electronic cooling equipment, etc., has not received enough attention. This observation motivates the present investigation. The main aim of this study is to carry out unsteady simulations of assisting mixed convective flow in a vertical channel with inclined plates attached to the active wall. It should be noted that this study is within the scope of previous works and aims to study the way to improve heat transfer in a vertical channel with inclined plates as vortex generators installed on the heated wall by using passive techniques, as these are economical and do not require any external additions. This method of improving heat transfer by changing the flow direction towards the walls and activating the self-sustained oscillatory flow using inclined plates can be used in the cooling air of electronic systems and heat exchangers because the passages in these systems are often narrow, and the flow velocity is usually low [7]; therefore, laminar flow simulations have been performed for low and intermediate Reynolds numbers in the range of 200 to 1400. The influence of operating parameters such as Reynolds number, Grashof number, and

geometric parameters such as plate tilt angle on heat transfer and flow behavior in steady-state flow as well as in self-sustained oscillatory flow under buoyancy effect was analyzed.

2. Model Description

2.1. Model Structure

The flow structure examined in this study is depicted in Fig. 1. It consists of a two-dimensional vertical channel with a length L and a width (H). Five adiabatic inclined plates with angle (γ) are regularly attached to the heated wall to investigate the laminar mixed convective flow. Each plate has a thickness of 0.02H. The dimensionless plate height, defined as (h_p=h/H= 0.3) corresponds to the blockage ratio for the channel width of unity. However, all the smooth walls remain adiabatic and the dimensionless plate spacing is $D = d/H$, which is equal to one. In this study, plate angles of γ = 30°, 60° and 90° are adopted to examine unsteady heat transfer behavior. Preheating (L_{in}) and post heating (L_{out}) lengths are carefully selected to prevent any unrealistic boundary conditions at the inlet and outlet. Therefore, Preheating, heating and post heating lengths are $L_{in} = 6H$, $L_h = 6H$ and $L_{out} = 12H$ respectively, as indicated in Fig.1. Therefore, the total channel length is L = 24H. A uniform upward airflow enters the channel from the bottom with a constant velocity and temperature (U_0, θ_0) and exits from the top of the channel. Thus, the convection occurs within the assisted flow regime. The fluid flow (air, Pr = 0.71) is assumed to be laminar, incompressible; the fluid is viscous, Newtonian; viscous dissipation and heat source terms are not taken into account in the energy equation. All thermo-physical properties of the fluid remain constant, except for the fluid density in the buoyancy term, where the Boussinesq approximation is adopted.

2.2. Governing Equations

Given the above assumptions, the governing Eqs. (1)-(4) of continuity, momentum, and temperature for unsteady two-dimensional mixed convection flow can be expressed in their dimensionless form as follows:

- Mass:

$$\frac{\partial U}{\partial X} + \frac{\partial V}{\partial Y} = 0 \qquad (1)$$

- X-momentum:

$$\frac{\partial U}{\partial \tau} + U\frac{\partial U}{\partial X} + V\frac{\partial U}{\partial Y} = \frac{-\partial P_m}{\partial X} + \frac{1}{Re}\left(\frac{\partial^2 U}{\partial X^2} + \frac{\partial^2 U}{\partial Y^2}\right) + \frac{Gr}{Re^2}\theta \qquad (2)$$

- Y-momentum:

$$\frac{\partial V}{\partial \tau} + U\frac{\partial V}{\partial X} + V\frac{\partial V}{\partial Y} = \frac{-\partial P_m}{\partial Y} + \frac{1}{Re}\left(\frac{\partial^2 V}{\partial X^2} + \frac{\partial^2 V}{\partial Y^2}\right) \qquad (3)$$

- Energy:

$$\frac{\partial \theta}{\partial \tau} + U\frac{\partial \theta}{\partial X} + V\frac{\partial \theta}{\partial Y} = \frac{1}{PrRe}\left(\frac{\partial^2 \theta}{\partial X^2} + \frac{\partial^2 \theta}{\partial Y^2}\right) \qquad (4)$$

These are the equations that describe the evolution of velocity and temperature fields over both space and time.

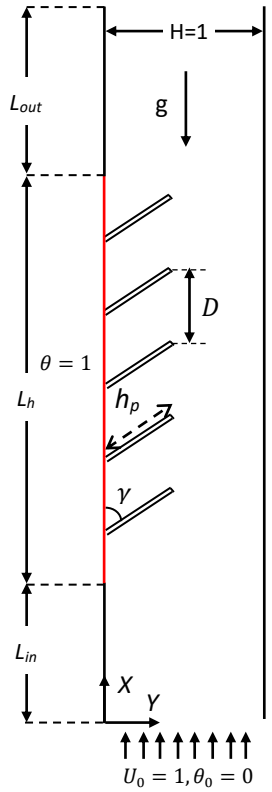

Fig. 1. Diagram of computational domain

The dimensionless variables used to derive the governing transport time-dependent equations mentioned earlier are defined as:

$$X = \frac{x}{H},\ Y = \frac{y}{H},\ U = \frac{u}{u_0},\ V = \frac{v}{u_0}$$
$$\tau = \frac{tu_0}{H},\ P_m = \frac{(p+\rho_0 gx)}{\rho_0 u_0^2},\ \theta = \frac{(T-T_0)}{(T_w-T_0)} \qquad (5)$$

where u and v represent the velocity components, x, y represent the Cartesian coordinates, p_0 the pressure, ρ_0 the density, T the temperature, and T_w is the wall temperature, H is the channel width, u_0 and T_0 represent the velocity and temperature at the inlet conditions, respectively. The subscript '0'refers to the inlet condition and 'w' refers to the wall.

The dimensionless parameters are the Reynolds number ($Re = u_0H/\nu$) which measures the ratio of inertial to viscous forces; the Grashof number ($Gr=g\beta(T_w-T_0)\ H^3/\nu^2$) which defines the

ratio of buoyancy to viscous forces acting on a fluid. The Prandtl number ($Pr = \nu/\alpha$) which defines the ratio of momentum and heat diffusion. Thus, Richardson number ($Ri = Gr/Re^2$), provides a measure of the influence of free convection (buoyancy forces) in comparison with the forced convection (inertial forces) and Péclet number ($Pe = Re\ Pr$) defines the ratio of inertial forces to thermal diffusivity. Here, $\nu = \frac{\mu}{\rho_0}$ is the kinematic viscosity and α is the thermal diffusivity ($\frac{k}{\rho_0 C_p}$).

2.3. Physical Quantities

Heat transfer is evaluated by the use of the local Nusselt number, which represents the ratio of convective heat transfer to pure conductive heat transfer in the fluid phase. The local Nusselt Number at the heated wall of the channel is defined as:

$$Nu_X = \frac{hH}{k} = \frac{\frac{-k\frac{\partial T}{\partial y}\Big|_w}{T_w - T_0} H}{k} = -\frac{\partial T}{\partial y}\Big|_w \frac{H}{T_w - T_0} = -\frac{\partial \theta}{\partial Y}\Big|_w \tag{6.a}$$

where h denotes the heat transfer coefficient determined by the local temperature gradient at the heated wall as follows:

$$h = \frac{-k\frac{\partial T}{\partial y}\Big|_w}{T_w - T_0} \tag{6.b}$$

The mean Nusselt number over the heated part of the channel is expressed as:

$$Nu = \frac{1}{L_h}\int_0^{L_h} Nu_X\, dX \tag{7}$$

For the unsteady flow, the time-averaged local Nusselt number by period is expressed as:

$$\overline{Nu}_X = \frac{1}{\tau_p}\int_0^{\tau_p} Nu_X\, d\tau \tag{8}$$

The time-averaged mean Nusselt number is given as:

$$Nu = \frac{1}{L_h}\int_0^{L_h} \overline{Nu}_X\, dX \tag{9}$$

The friction factor is determined using the pressure drop (Δp) across the dimensionless length of the heated part of the channel (L_h) as:

$$f = \frac{2\,\Delta p H}{\rho_0 u_0^2 l_h} = \frac{2\,\Delta p}{\rho_0 u_0^2 \frac{l_h}{H}} = \frac{2\,\Delta p}{\rho_0 u_0^2 L_h} \tag{10}$$

The performance factor is defined as the ratio of heat transfer enhancement (Nu/Nu_s) to the increase in flow energy (f/f_s). It is determined using the following expression:

$$\eta = \frac{{}^{\mathrm{Nu}}/_{\mathrm{Nu_s}}}{{}^{f}/_{f_s}} \tag{11}$$

where Nu_s and f_s represent the Nusselt number and the friction factor for the channel without plates.

The Strouhal number, which characterizes the oscillatory behavior of the fluid flow, is defined as follows:

$$St = \frac{FH}{u_0} \tag{12}$$

where F is the dimensional frequency or the vortex shedding frequency.

2.4. Boundary Conditions

At the inlet channel, the flow has a uniform velocity ($U_0 = 1$) and a constant temperature ($\theta_0 = 0$) as the inlet condition, with a zero gradient for pressure. At the outlet channel, a zero gradient of the physical quantities (U, V and θ) is maintained along with atmospheric pressure ($P_m = 0$). At the plates surfaces and the channel walls, the typical no-slip condition ($U = V = 0$) is used. The first plate is positioned at 7 H from the inlet to allow for the development of the velocity profile, while the last one is located at 13H from the outlet. This placement ensures that the reattachment point after the recirculation zone downstream of the last plate is included within the computational domain and prevents any influence from the inlet and outlet on the physical quantities being studied. The heated wall of the channel is maintained at a constant temperature ($\theta_w = 1$), while all other channel walls are kept adiabatic.

3. Solution Method

The governing transport equations (1)-(4) and their associated boundary conditions presented previously were solved using OpenFOAM®, an open-source code built on the finite volume formulation. The PIMPLE (Pressure-Implicit Method for Pressure Linked Equation) algorithm, which combines the SIMPLE and PISO algorithms introduced by Patankar [37], is used to couple velocity-pressure fields. All the governing equations (1) – (4) are discretized with a second–order implicit scheme for the time integration. To discretize the spatial domain, second–order schemes are used to compute the gradient, divergence, and Laplacian terms. The simulation is validated by comparing it with the pertinent experimental data of Armaly et al. [38] for the laminar separated flow occurring in a backward-facing step at $X = 0$ and Re = 100.

The results show good conformity, with the maximum difference does not exceed 0.5%, as shown in Figure 2(a). Further, the simulation of an inclined surface with a uniform wall heat flux for laminar mixed convective flow was carried out at ζ =1.31. Here, ζ is the buoyancy parameter, defined as $(g\beta q_w x^4)/(u_0 x/\nu)^{2.5}$ in [39], where q_w and x are the wall heat flux and the longitudinal location, respectively. The distribution of the dimensionless temperature is depicted in Figure 2(b). Very good agreement between the current numerical simulation and the experimental data of Abu-Mulaweh [39] was observed.

To check the independence of the results from the grid resolution. A typical case of unsteady flow (Re = 1400, Gr = 2×10^5, h_p = 0.3 and γ = 90°) has been examined. A series of simulations was performed using four different mesh configurations (300×60, 400×80, 500×100 and 600×120). Table 1 shows a change of less than 0.2% in the time-averaged mean Nusselt number between the two last mesh sizes. Hence, the grid size of 500×100 has been chosen adequate for all simulations of flow and thermal gradient throughout the current study and offers a favorable balance between computational cost and precision. In this work, the time-dependent computations are begun with the fluid at rest, and a small dimensionless time step (Δτ = 0.002) is used for all simulations. This ensures that the maximum Courant number in the flow field remains less than 0.5. It is noted that the time step relies on the configuration and flow velocity to precisely capture the intricate unsteady flow. Calculations are considered complete when all residuals for mass, momentum and energy equations fall below 10^{-7}.

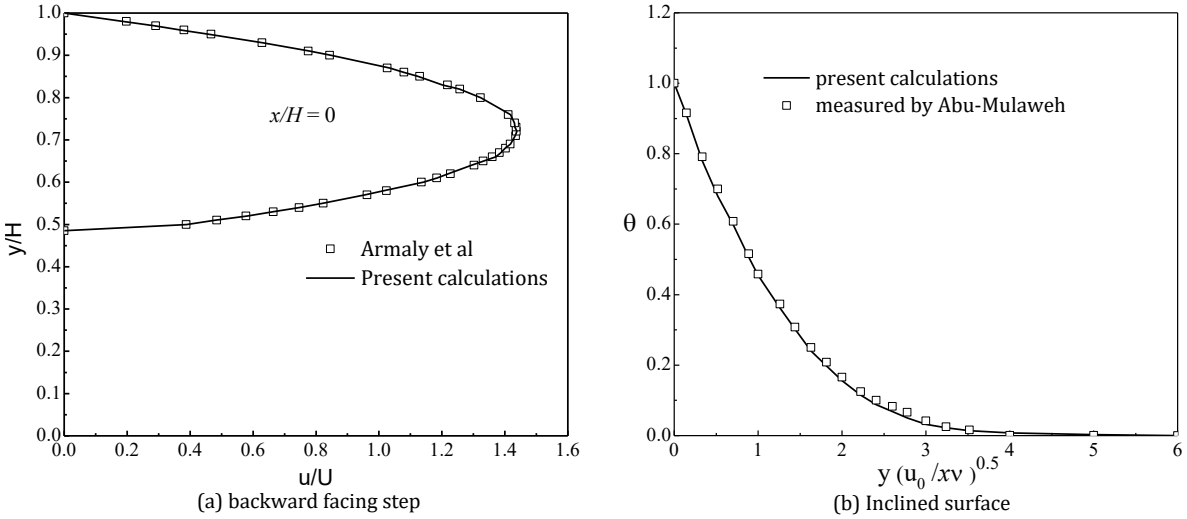

(a) backward facing step (b) Inclined surface

Fig. 2. Comparison of velocity profile and dimensionless temperature for backward facing step and inclined surface

Table 1. Effect of grid on the mean Nusselt Number at Re = 1400, Gr = 2 10^5 and h_p = 0.3

Grid	60×300	80×400	100×500	120×600
Nu	14.29	14.38	14.44	14.47

4. Results and Discussions

In this study, the dimensionless parameters that characterize the flow field and heat transfer behavior in a vertical channel are: the Reynolds number defined as a function of the channel width is in the range of 200 to 1400, while the Grashof number takes two values, 10^5 and 2×10^5. For the geometric configuration, calculations were performed for a blockage ratio or plate height of h_p = 0.3. However, the distance between two adjacent plates is assumed to be constant (D = d/H =1). To study the effect of inclined plates in the flow direction, three angles of inclination γ = 30°, 60°, and 90° were used. The thickness of the plates is not included as an additional parameter in the flow field analysis because it is considered negligible in relation to the plate spacing. A series of numerical computations was performed under unsteady conditions until either steady-state flow or periodic/chaotic flow is achieved. The effect of inclined plates is examined a crossdiverse combinations of Reynolds number (Re) and Grashof number (Gr) to gather quantitative

insights into different flow structures. These combinations provide Richardson number (*Ri*) between 0.1 and 5 to simultaneously account for both buoyancy and inertial effects. Particular focus was given to the analysis of flow structure and heat transfer features within the studied Reynolds number range to avoid the onset of turbulent flow.

4.1. Flow Patterns and Thermal Behavoir

Figure 3 presents the streamline patterns for different plate tilt angles (γ = 30, 60, and 90°) at *Re* = 600, *Gr* = 10^5, and h_p = 0.3. These figures illustrate that the dimensions of the recirculation zones behind each plate are relatively increase as γ increases. Additionally, for γ = 90°, a smaller secondary recirculation zone is observed on the opposite side of the larger vortex formed behind the last plate. This secondary recirculation zone arises from the rapid change in axial velocity on the opposite side after the last plate, leading to an unfavorable positive pressure gradient. Consequently, this recirculation zone produces a significant pressure drop due to the reduced velocity gradient near the right wall in the secondary backflow region.

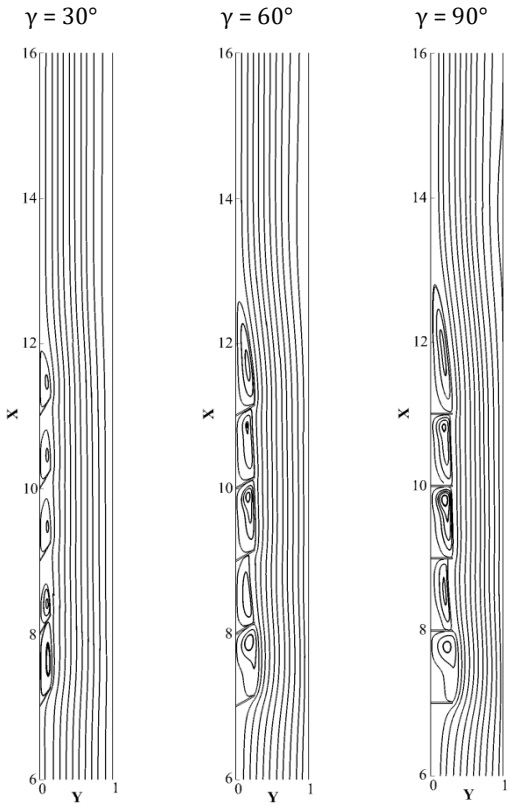

Fig. 3. Streamlines at *Re* = 600, *Gr* = 10^5 and h_p = 0.3 for various plate tilt angles γ.

Figure 4 displays the corresponding dimensionless isotherm contours. As the tilt angle of the plates increases, the density of the isotherm contours at the reattachment point also increases, leading to an increase in the thermal gradient and consequently an improvement in heat transfer. Conversely, as the tilt angle of the plates decreases, the isotherm contours at the reattachment point become sparser, leading to a reduced thermal gradient and a lower heat transfer rate. Additionally, the recirculation zones behind each plate are confined, directing the fluid near the wall toward the core flow, allowing heat to diffuse away and be evacuated to the outlet.

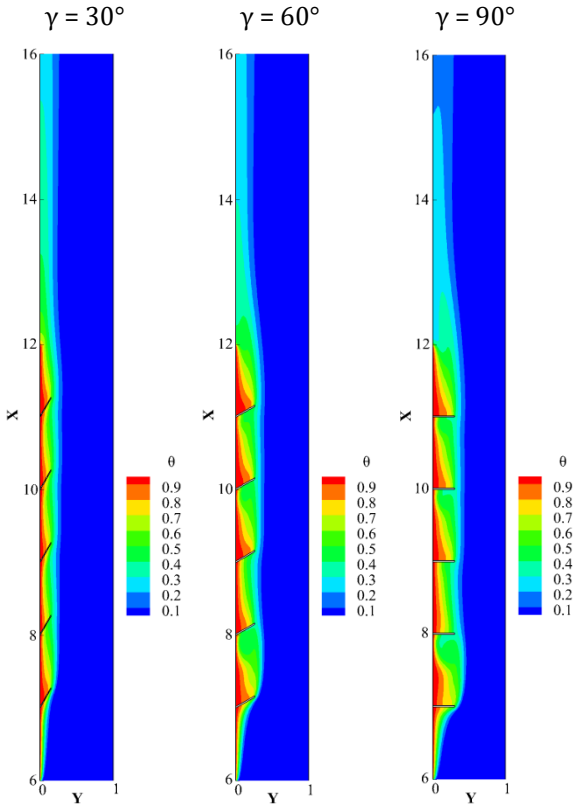

Fig. 4. Thermal patterns at *Re* = 600, *Gr* = 10^5 and h_p = 0.3 for various plate tilt angles γ.

Figure 5 illustrates the flow structure for three Reynolds number values (200, 400, and 600) at *Gr* = 10^5 and h_p = 0.3. From the figure, it is evident that the flow exhibits steady-state behavior, with streamlines remaining parallel throughout the entire channel, except in the regions situated before and after the plates, where a backflow zone develops due to the pressure variation resulting from the abrupt change in passage section. In addition, the vortices are sharper and more concentrated directly behind each plate. This happens because the plates obstruct the fluid flow, which restricts the recirculating region from extending further downstream of each plate.

At low Reynolds number (Re = 200), the vortices are smaller and adopt an oval shape. These vortices are increasingly influenced by the

main flow and become larger as the Reynolds number increases. The length of these vortices increased as the Reynolds number increased, particularly for the one located behind the last plate, due to the lack of specific constraints. In this Reynolds number range and at a constant Grashof number, buoyant forces dominate the flow and cause it to circulate around the plates before entering the cavity locations. As the Reynolds number increases, inertial forces become more pronounced and inhibit the main flow from entering between the plates. In addition, behind each plate, the vortices are steeper and more densely packed. This behavior is expected because the plates act as impermeable barriers to the fluid flow, which causes the recirculation zones to remain concentrated near the plates and not be blown farther downstream of every plate.

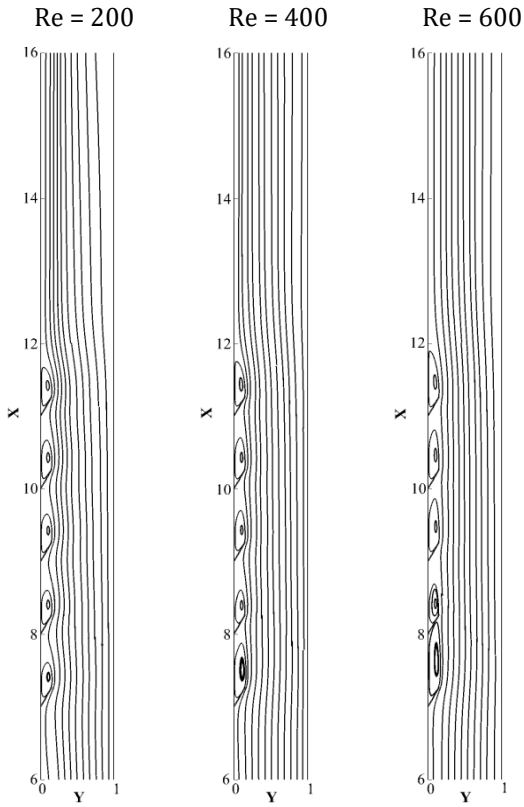

Fig. 5. Streamlines versus Reynolds number at $Gr = 10^5$, $hp = 0.3$ and $\gamma = 30°$

The isotherm contours under the identical conditions are depicted in Figure 6. This figure shows that the addition of plates alters the flow structure and thermal patterns. Consequently, the flow velocity profile is disrupted by the plates. The vortices formed by the backflow zones after each plate consist of almost the same fluid particles; So they act effectively as stagnation regions that trap and insulate the warm fluid. In these low-velocity areas, the heat transfer is occurred mainly by diffusion, showed by a low Nusselt number. At the reattachment point, the isotherms become compressed and represented by a thin near-wall layer. This thin near- wall layer increases the temperature gradient, which leads to an increase in Nusselt number. As the Reynolds number increases, the isotherms extend further downstream behind each plate. This is because at high Re, thermal diffusion remains significant relative to the convective heat transfer, which contributes noticeably to the overall heat transport.

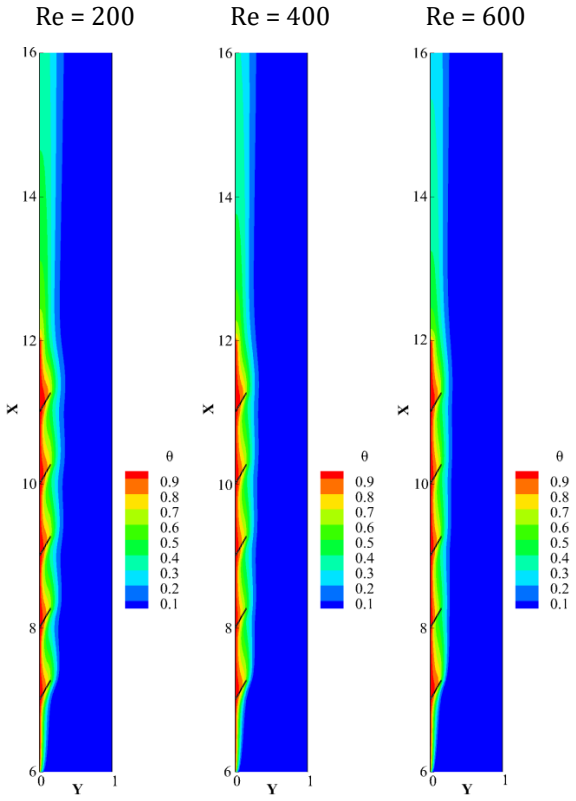

Fig. 6. Isotherm contours versus Reynolds number at $Gr = 10^5$, $hp = 0.3$ and $\gamma = 30°$

As shown by the previous illustrations (Figures 5 and 6), the flow is in a steady state at low Reynolds number, even though the calculations are performed using an unsteady scheme. The time–velocity history at a control point ($X = 11.5$, $Y = 0.5$) for the case of $Re = 600$ and $Gr = 10^5$ reveals that the flow velocity oscillates before converging to a stable value, as depicted in Figure 7(a). The steady state disappears at $Re > Re_c$, and the flow translates to the unsteady regime, and a self-sustained oscillatory flow settles down.

The unsteadiness increases as the Reynolds number increases. The results indicate that the unsteady state exhibits a time-periodic self-sustained oscillatory flow. At Reynolds numbers exceeding the critical value ($Re > Re_c$), the flow becomes unsteady and undergoes periodic oscillations over time. This behavior is evident in

the time evolution of the U-velocity component at the control point, where the velocity asymptotically converges to a periodic state with the same oscillatory amplitude after a certain elapsed time, as illustrated in Figure 7(b).

This oscillatory flow is induced by the initiation of Tollmien–Schlichting waves activated by Kelvin–Helmholtz shear-layer instabilities spanning the plates, caused by the periodic contraction and expansion of the flow due to the geometric topology. In addition, this phenomenon is driven by the continuous rotation and deformation of vortices along the walls. Notably, the dimensionless time period, τ_p, is approximately 1.02 units.

The Fast Fourier Transform (FFT) diagram of the U-velocity component time evolution is plotted in Figure 8 at Re = 1200, Gr = 10^5, γ = 30°, and h_p = 0.3. One can see a single fundamental dominant non-dimensional frequency wave with St = 0.973, where $St = FH/u$. is the Strouhal number.

The Strouhal number quantifies the balance between inertial forces from local flow acceleration and those from convective acceleration. In simpler terms, it represents the dimensionless frequency at which vortices are shed. A harmonic frequency with low amplitude is observed. This harmonic frequency corresponds to the combination of two Tollmien–Schlichting waves. However, the dimensionless frequency of the oscillatory flow is associated with the traveling Tollmien–Schlichting wave. One harmonic can be identified. The amplitude of this harmonic is just to the right of the fundamental frequency. Ultimately, it should be noted that the precise value of the critical Reynolds number (Re_c) that corresponds to the transition from the steady state to the unsteady state is not considered in this study; it seems that Re_c is highly dependent on plate tilt angle and flow velocity. An exact value would be difficult task and requires a special technique like linear stability analysis.

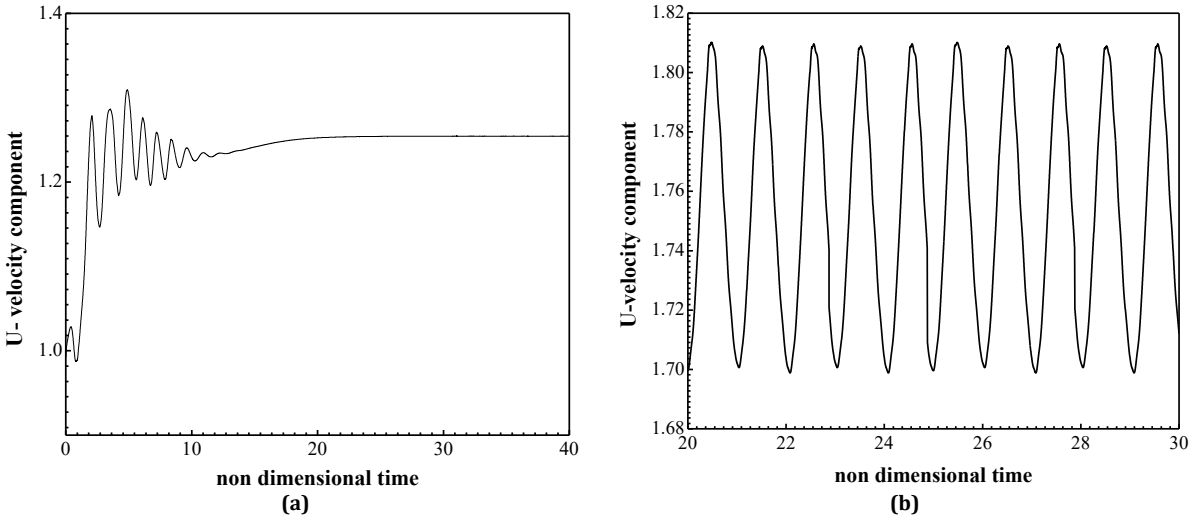

Fig. 7. Time history of the U-velocity component at the reference point (X =11.5, Y = 0.5) for Gr = 10^5, h_p= 0.3 and (a) Re =600 and (b) Re =1200

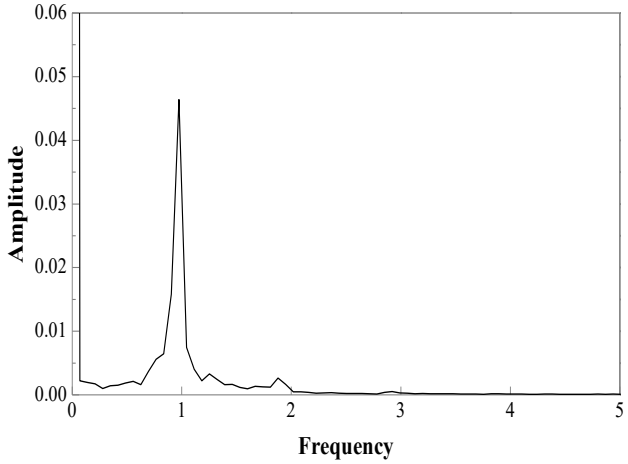

Fig. 8. FFT analysis of the U-velocity component history for Re =1200, Gr =10^5, h_p = 0.3 and γ=30°

4.2. Effect of Reynolds and Grashof Numbers

Heat transfer rate is quantified by calculating the local Nusselt number along the heated part for various combinations of Reynolds and Grashof numbers. Furthermore, the time-averaged mean Nusselt number is evaluated versus the Reynolds/Grashof number for each configuration.

The mean Nusselt number ratio Nu/Nu_s versus Reynolds number for h_p = 0.3 at different baffle tilt angles (γ = 30, 60, and 90°) and two Grashof number values is depicted in Figures 9(a)–9(c), where Nu_s represents the mean Nusselt number for a channel with no plates. These figures show that the heat transfer rate in steady-state flow, which occurs at low Reynolds number and across all Grashof numbers, can reach values of 1.05, 1.1, and 1.15 for γ = 30°, 60°, and 90°, respectively. In unsteady flow, a significant increase in heat transfer is observed and can attain 1.18, 1.54, and 1.6 at high Reynolds number for γ = 30°, 60°, and 90°, respectively. Notably, the improvement in heat transfer is more pronounced at low Grashof number due to the weaker influence of buoyancy forces relative to inertial forces. Nearthe plates, the flow velocity increases, which induces more interaction between the main flow and the plates. Thus, the residence time of fluid particles is reduced, leading to a greater decrease in its temperature gradient.

This reduction in the fluid temperature enhances heat transfer in these areas. Due to the slow flow velocity and the stronger buoyancy forces at high Grashof number, the aiding flow near to and just below the plates disrupts the main flow from coming into direct contact with the heated surface. In unsteady flow, heat transfer enhancement is the result of the continuous disruption and deformation of the boundary layer caused by flow oscillations. This effect is more intense as the Reynolds number increases. The emergence of self-sustained waves further improves fluid mixing, which in turn reduces the temperature near the heated wall.

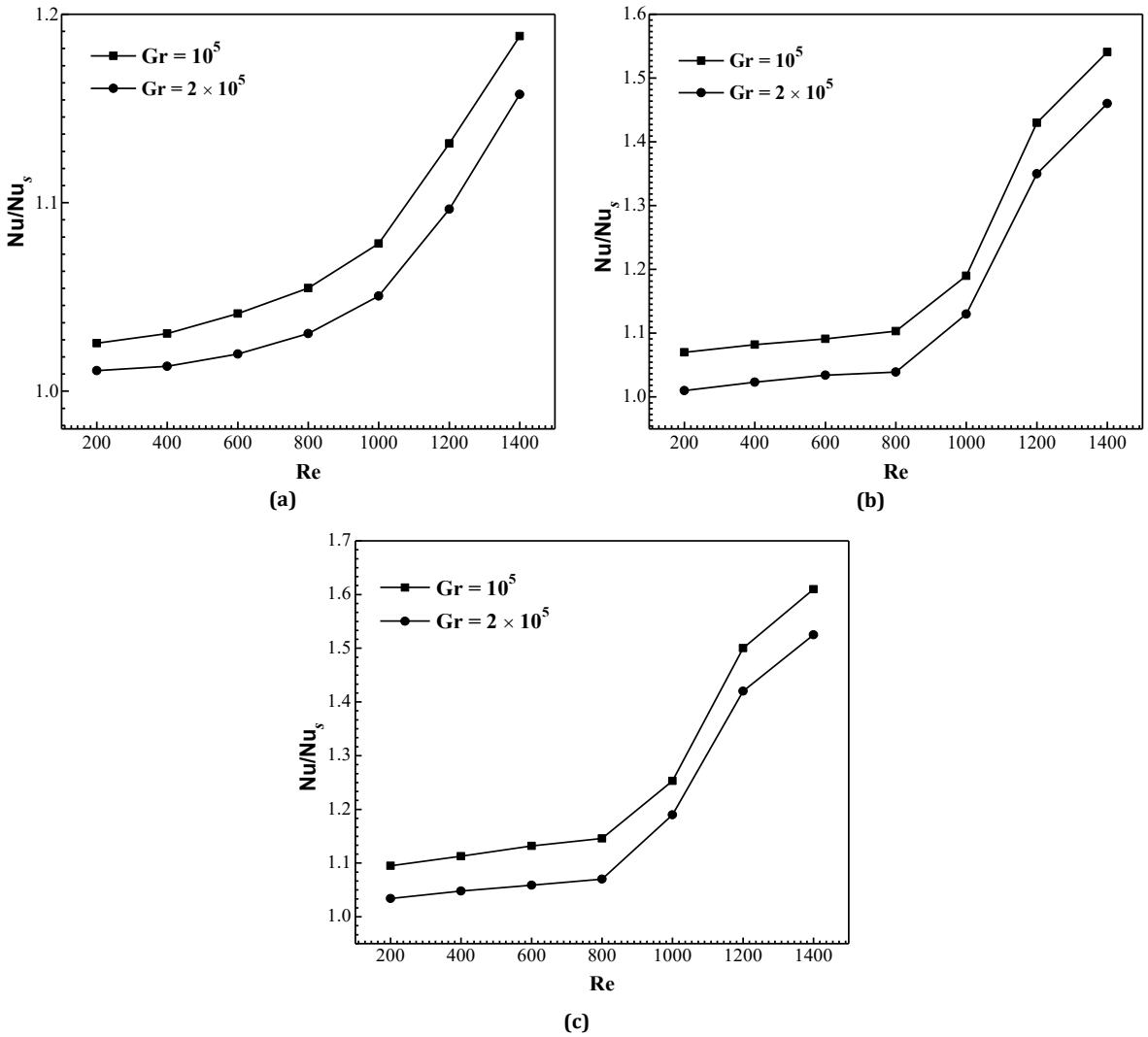

Fig. 9. Variation of Nusselt Number ratio versus *Re*for h_p= 0.3 and various Grashof numbers: (a) γ = 30°, (b) γ = 60° and (c) γ =90°.

As stated in the literature, the improvement of heat transfer results in increased energy flow. Consequently, a higher heat transfer rate is associated with greater pressure loss. Therefore, to quantify the flow energy required in this context, the variation in the friction factor ratio (f/f_s) is presented under identical conditions in Figures 10(a)–10(c).

These figures indicate that the friction factor ratio (f/f_s) increases as the Reynolds number increases, while it decreases as the Grashof number increases. At high Reynolds number, the ratio (f/f_s) can reach 2.4, 4.7, and 5.4 times for γ = 30, 60 and 90°, respectively, compared with the channel without plates. The use of plates enhances fluid mixing in the boundary layer but also involves more interactions between fluid and plates, as well as among the fluid particles. As a result, there is a higher pressure drop. At high Grashof number, the reduction in the friction factor is attributed to the buoyancy forces, which help to diminish flow interactions and reduce the friction factor even at high Reynolds number.

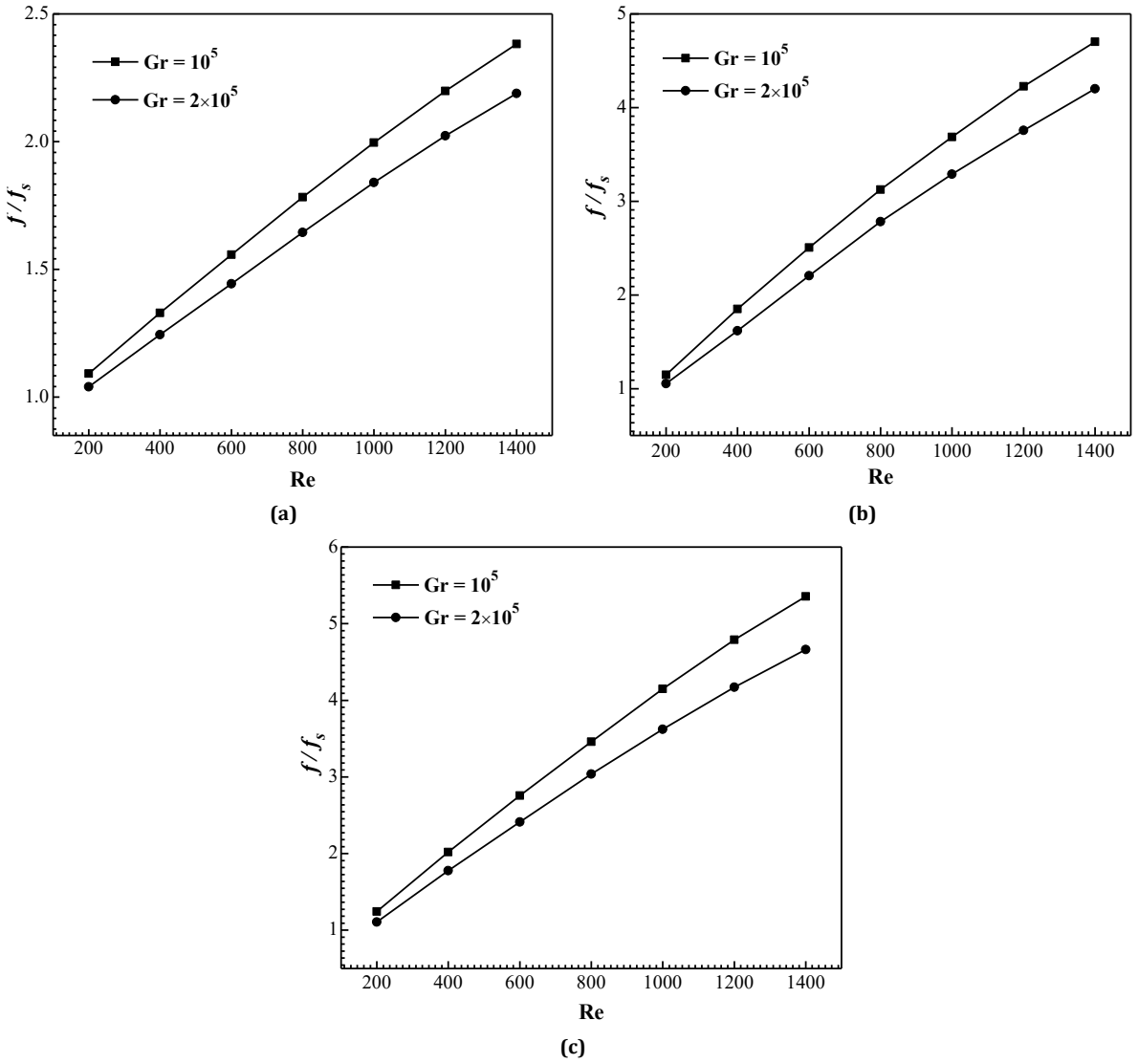

Fig. 10. Variation of friction factor ratio versus *Re* for h_p= 0.3 and various Grashof numbers: (a) γ = 30°, (b) γ = 60° and (c) γ=90°

4.3. Effect of Plate Tilt Angle

To have a clear and comprehensive insight into the impact of plate tilt angle on heat transfer efficiency, a series of calculations was conducted for various geometric configurations under various combinations of Reynolds and Grashof numbers. Figure 11 illustrates the variation of mean Nusselt number and friction factor ratios for different plate tilt angles at $Gr = 2 \times 10^5$ and $h_p = 0.3$. The mean Nusselt number ratio increases as both Reynolds number and plate tilt angle increase. The flow remains in a steady-state condition at low Reynolds number for all plate tilt angles, with only a slight augmentation in heat transfer observed. However, as the Reynolds number increases, an unsteady flow regime occurs,

which is characterized by self-sustained oscillations whose intensity depends on the Reynolds number. This oscillatory behavior significantly enhances heat transfer, which can reach 1.5 times for γ = 90° and Re = 1400, as shown in Figure 11(a).

The friction factor ratio (f/f_s) is presented in Figure 11(b). As shown in this figure, this ratio tends to increase as both Reynolds number and plate tilt angle increase. It is found to be about 1 to 4.6 times that of the channel without plates, for example, at γ = 90°. In addition, the results indicate that the (f/f_s) ratio is strongly influenced by both the Reynolds number and plate tilt angle. According to these results, it can be concluded that the presence of plates with larger tilt angles plays a vital role in causing an increase in flow energy.

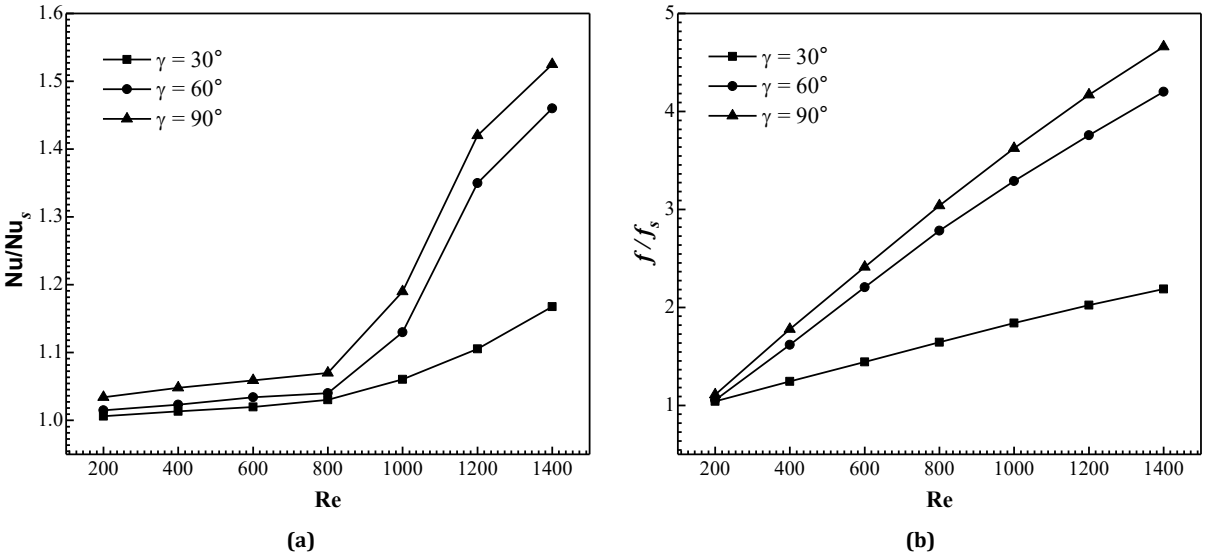

Fig. 11. Variation of: (a) Nusselt number ratio and (b) friction factor ratio versus *Re* at $Gr = 2\times10^5$ and various plate tilt angles

4.4. Performance Factor

In this work, the performance factor η is defined as the ratio of heat transfer improvement Nu/Nu_s to the increase in flow energy (f/f_s).

Figure 12 illustrates the variation of η with the Reynolds number for different plate tilt angles and two Grashof number values ($Gr = 2 \times 10^5$ and $Gr = 10^5$).

As indicated by this figure, the performance factor is high at low Reynolds numbers for all plate tilt angles. However, as the Reynolds number increases, a significant pressure drop occurs for all plate tilt angles, leading to a decrease in the performance factor.

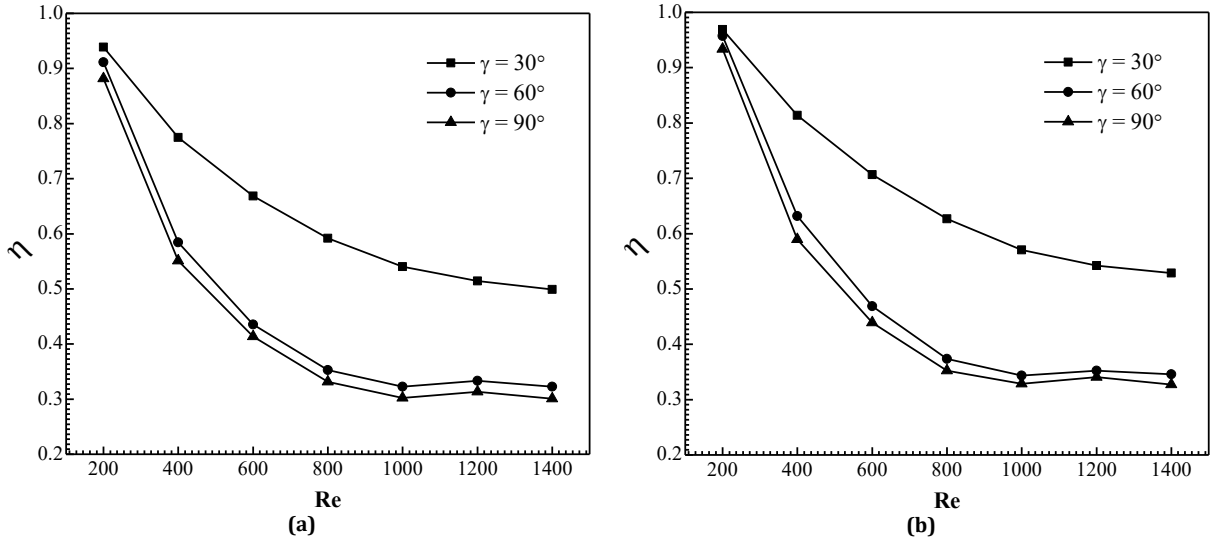

Fig. 12. Performance factor η versus *Re* at various plate tilt angles: (a) $Gr = 10^5$ and (b) $Gr = 2\times10^5$

The performance factor also decreases as the plate tilt angle increases due to the negative impact of the recirculation zone that forms downstream of the heated section. In addition, this negative impact increases as the Reynolds number increases and as the plate tilt angle increases.

As a result, the friction factor increases, and a decline in the performance factor is observed. Then, the performance factor increases as the plate tilt angle decreases. Finally, it can be concluded that a plate tilt angle of γ = 30° achieves a favorable balance between enhancing heat transfer and reducing flow energy.

5. Conclusions

Numerical simulations of laminar fluid flow and heat transfer in a vertical channel with five identical plates regularly distributed on the heated wall were carried out for $200 \leq Re \leq 1400$ and two values of the Grashof number $Gr = 10^5$ and 2×10^5. This investigation particularly highlights the improvement of heat transfer by modifying the direction of the flow towards the wall to be cooled and by activating self-sustained oscillatory flow using periodically placed plates. The effects of Reynolds number, Grashof number, and plate tilt angle at a constant plate height were examined. Streamlines and temperature contours were analyzed for different combinations of Reynolds and Grashof numbers. In addition, heat transfer and friction factor were examined based on plate tilt angles, Reynolds and Grashof numbers. The key findings of this study are summarized as follows:

- The flow develops into a self-sustained oscillatory pattern at moderate Reynolds number values. These values depend on the plate tilt angle.
- The Nusselt number and friction factor ratios increase as the Reynolds number increases, but decrease as the Grashof number increases.
- The heat transfer rate can be up to 1.15 times greater for steady-state flow and 1.6 times greater for unsteady flow when compared to a channel without plates at high plate tilted angle and low Grashof number.
- An improve in heat transfer rate can reach up to 15%, 45% and 50% in terms of the Nusselt number for γ = 30°, 60° and 90°, respectively, at high Reynolds number and high Grashof number.
- The performance factor improves with the Grashof number but declines with the Reynolds number and plate tilt angle.
- The performance factor reaches up to 52%, 34% and 31% for γ = 30°, 60° and 90°, respectively.
- The plate tilt angle γ = 30° provides an optimal balance between the heat transfer improvement and the reduction in flow energy.

Nomenclature

C_p	Specific heat of air, J/kg.K
d	Plate distance, m
D	Dimensionless plate distance, $D = d/H$ =1
f	Friction factor, $f=2\Delta p/\rho_0 u_0^2 L$
f_s	Friction factor in smooth channel
F	Dimensional frequency, Hz
h	Plate height, m
H	Channel width, m
h_p	Dimensionless baffle height or blockage ratio, $h_p = h/H$
K	Thermal conductivity, W/m.K
L_h	Dimensionless heated part length [$L_h = \frac{l_h}{H}$]
L_{in}	Dimensionless inlet length, $L_{in} = \frac{l_{in}}{H}$
L_{out}	Dimensionless outlet length, $L_{out} = \frac{l_{out}}{H}$
Nu_X	Local Nusselt number
$\overline{Nu}_X$	Time-averaged local Nusselt number by period
Nu	Mean Nusselt number
Nu_s	Mean Nusselt number in smooth channel
p	Pressure, Pa
P_m	Dimensionless pressure, $P_m = (p + \rho_0 g x)/\rho_0 u_0^2$
Δp	Pressure drop, Pa
Pr	Prandtl number, $Pr = \nu/\alpha$

Re	Reynolds number, $Re = u_0 H/\nu$
Re_c	Critical Reynolds number
St	Strouhal number, $St = FH/u_0$
T	Temperature, K
t	Time, s
u, v	Velocity components in x and y-directions, m/s
U, V	Dimensionless velocity components, $U = \frac{u}{u_0}, V = \frac{v}{u_0}$
x, y	Dimensional Cartesian coordinates, m
X,Y	Dimensionless Cartesian coordinates, $X = x/H, Y = y/H$

Greek letters

α	Thermal diffusivity of air, m^2/s
β	Thermal expansion coefficient, $1/K$
γ	Plate tilt angle
Δ	Difference
$\Delta\tau$	Time step
η	Performance factor, $(Nu/Nu_s)/(f/f_s)$
θ	Dimensionless temperature, $\theta = (T - T_0)/(T_w - T_0)$
μ	Dynamic viscosity of air, kg/s.m
ν	Kinematic viscosity of air, m^2/s
ρ	Density of air, kg/m^3
τ	Dimensionless time, $\tau = tu_0/H$

Subscripts

0	At inlet conditions
p	Refers to one period
s	Smooth channel
w	Wall

Funding Statement

This research did not receive any specific grant from funding agencies in the public, commercial, or not-for-profit sectors.

Conflicts of Interest

The author declares that there is no conflict of interest regarding the publication of this article.

Authors Contribution Statement

Nabila Trad: Investigation; Data Curation; Methodology; Software; Validation; Writing – Original Draft.

Rabah Henniche: Conceptualization; Project administration; Supervision; Writing – Original Draft; Writing – Review & Editing.

Abdelkader Korichi: Conceptualization; Formal Analysis; Investigation; Methodology; Validation.

References

[1] Valencia, A., 1996. Unsteady flow and heat transfer in a channel with a built-in tandem of rectangular cylinders. *Numerical Heat Transfer, Part A: Applications*, 29(6), pp. 613–623.

[2] Ishino, Y., Suzuki, M., Abe, T., Ohiwa, N., Yamaguchi, S., 1996. Flow and heat transfer characteristics in pulsating pipe flows (effects of pulsation on internal heat transfer in a circular pipe flow).*Heat Transfer–Japanese Research,* 25(5), pp. 323–341.

[3] Guo, J., Fan, A., Zhang, X., Liu, W., 2011. A numerical study on heat transfer and friction factor characteristics of laminar flow in a circular tube fitted with center-cleared twisted tape. *International Journal of Thermal Sciences*, 50, pp. 1263-1270.

[4] Korichi, A., Oufer, L., Polidori, G., 2009. Heat transfer enhancement in self-sustained oscillatory flow in a grooved channel with oblique plates. *International Journal of heat and mass transfer*, 52, pp. 1138–1148.

[5] Garimella, S.V., Eibeck, P.A., 1990. Heat transfer characteristics of an array of protruding elements in single phase forced convection. *International Journal of heat and mass transfer*, 33(12) pp. 2659-2669

[6] Roberts, E. P. L., 1994. A numerical and experimental study of transition processes in an obstructed channel flow. *Journal of Fluid Mechanics*, 260, pp. 185–209.

[7] Wang, G., Stone, K., and Vanka, S. P., 1996. Unsteady heat transfer in baffled channels. *Journal of Heat Transfer*, 118 (3), pp. 585–591.

[8] Yuna, Z.X., Tao, W.Q., Wang, Q., 1999. Experimental investigation of heat transfer enhancement in ducts with winglet fins. *First International Conference of Engineering Thermophysics, Beijing, China*, pp. 457–463.

[9] Fu, W.S., Tong, B.H., 2004. Numerical investigation of heat transfer characteristics of the heated blocks in the channel with a transversely oscillating cylinder. *International Journal of heat and mass transfer*, 47(2), pp. 341-351.

[10] Mousavi, S.S., Hooman, K., 2006. Heat and fluid flow in entrance region of a channel with staggered baffles. *Energy Conversion and Management*, 47(15-16), pp. 2011–2019.

[11] Ko, K. H., Anand, N. K., 2003. Use of porous baffles to enhance heat transfer in a rectangular channel. *International Journal of Heat and Mass Transfer*, 46(22), pp. 4191–4199.

[12] Guzman, A. M., Del Valle, M., 2006. Heat transfer enhancement in grooved channels due to flow bifurcations. *Heat and Mass Transfer*, 42(11), pp. 967–975.

[13] Fu, W. L., Wright, L. M., Han, J. C., 2006. Heat transfer in two-pass rotating rectangular channels (AR _ 2:1) with discrete ribs. *Journal of Thermophysics and Heat Transfer*, 20(3), pp. 569–582.

[14] Liu, Y. H., Wright, L.M., Fu, W.L., Han, J.C., 2007. Rib spacing effect on heat transfer in rotating two-Pass ribbed channel (AR =1:2). *Journal of Thermophysics and Heat Transfer*, 21(3), pp. 582–595.

[15] Wright, L. M., Gohardani, A. S., 2009. Effect of coolant ejection in rectangular and trapezoidal trailing-edge cooling passages, *Journal of Thermophysics and Heat Transfer*, 23(2), pp. 316–326.

[16] Santos, N. B., de Lemos, M. J. S., 2006. Flow and heat transfer in a parallel-Plate channel with porous and solid baffles. *Numerical Heat Transfer, Part A: Applications*, 49(5), pp. 471–494.

[17] Zhang, H. J., Zou, Z. P., Shao, F., Song, S. H., 2015. Investigations of heat transfer enhancement in a channel with staggered porous ribs by the preconditioned density-based algorithm. *Numerical Heat Transfer, Part A: Applications*, 67(12), pp. 1370–1385.

[18] Promvonge, P., Jedsadaratanachai, W., Kwankaomeng, S., 2010. Numerical study of laminar flow and heat transfer in square channel with 30° inline angled baffle turbulators. *Applied Thermal Engineering*, 30(11–12), pp. 1292–1303.

[19] Promvonge, P., Sripattanapipat, S., Kwankaomeng, S., 2010. Laminar periodic flow and heat transfer in square channel with 45° inline baffles on two opposite walls. *International Journal of Thermal Sciences*, 49(6), pp. 963–975.

[20] Peng, W., Jiang, P. X., Wang, Y. P., Wei, B. Y., 2011. Experimental and numerical investigation of convection heat transfer in channels with different types of ribs. *Applied Thermal Engineering*, 31(14–15), pp. 2702–2708.

[21] Lopez, J.R., Anand, N.K., Fletcher, L.S., 1996. Heat Transfer in a Three-dimensional channel with baffles. *Numerical Heat Transfer, Part A: Applications*, 30(2), pp. 189–205.

[22] Guo, Z., Anand, N.K., 1997. Three-dimensional heat transfer in a channel with a baffle in the entrance region. *Numerical Heat Transfer, Part A: Applications*, 31(1), pp. 21–35.

[23] Tsay, Y.L., Chang, T.S., Cheng, J.C., 2005. Heat transfer enhancement of backward-facing step flow in a channel by using baffle installation on the channel wall, Acta Mechanica, 174(1-2), pp. 63–76.

[24] Bazdidi-Tehrani, F., Naderi-Abadi, M., 2004. Numerical analysis of laminar heat transfer in entrance region of a horizontal channel with transverse fins. *International Communications in Heat and Mass Transfer*, 31(2), pp. 211– 220.

[25] Cheng, C.H., Luy, C.D., Huang, W.H., 1992. Buoyancy effect on the heat convection in vertical channels with fin array at low Reynolds numbers. *International Journal of heat and mass transfer*, 35(10), pp. 2643–2653.

[26] Cheng, C.H. Yang, J.J., 1994. Buoyancy-induced recirculation bubbles and heat convection of developing flow in vertical channels with fin arrays.*International Journal of Heat and Fluid Flow*, 15(1), pp. 11–19, 1994.

[27] H.C. Fung, H.C., Lazaridis, A., 1996. Mixed convection of laminar, fully-developed flow

in a finned channel. *WIT Transactions on Engineering Sciences*, 12, pp. 3–12.

[28] Chang, T.S., Shiau, Y.H., 2005. Flow pulsation and baffle's effects on the opposing mixed convection in a vertical channel. *International Journal of heat and mass transfer*, 48(20), pp. 4190-4204.

[29] Fu, W.S., Huang, J.C., Wang, Y.Y., Huang, Y., 2013. Enhancement of heat transfer of mixing convection in a vertical channel by a moving block. *Journal of Mechanics*, 29(1), pp. 95–107.

[30] Nemitallah, M. A., Zohir, A. E., 2016. Investigations of heat transfer, entropy generation and pressure build up for upward flow in a vertical channel equipped with a fin array. *Heat and Mass Transfer*, 52(9), pp. 1953–1961.

[31] Chang, T.S., 2015. Enhanced three-dimensional mixed convection in a horizontal channel using a baffle. *Heat Transfer Engineering*, 36(17), pp. 1426–1435.

[32] Henniche, R., Korichi, A., 2017. Heat transfer enhancement in self-sustained oscillatory flow in a staggered baffled vertical channel under the buoyancy effect. *Numerical Heat Transfer, Part A: Applications*, 71(12), pp.1189-1204.

[33] Kumar, A., Kumar, R., Maithani, R., Chauhan, R., Kumar, S., Nadda, R., 2017. An experimental study of heat transfer enhancement in an air channel with broken multi type V-baffles. *Heat and Mass Transfer*, 53, pp. 3593-3612.

[34] El Habet, M.A., Ahmed, S.A., Saleh, M.A., 2021. Thermal/hydraulic characteristics of a rectangular channel with inline/staggered perforated baffles. *International Communications in Heat and Mass Transfer*, 128, 105591.

[35] Kurian, S., Tide, P.S., Biju, N., 2021. Effect of baffle configuration on heat transfer and pressure drop characteristics of jet impingement system with cross-flow. *Journal of Advanced Research in Fluid Mechanics and Thermal Sciences*, 86(2), pp. 15-27.

[36] Henniche, R., Korichi, A., 2025.Mixed and forced convection heat transfer in baffled channels: A brief review. *Journal of Heat and Mass Transfer Research*, 12(1), pp. 15-28.

[37] Patankar, S.V., 1980. Numerical heat transfer and fluid flow, New York: Hemisphere Publishing Corporation.

[38] Armaly, B.F., Durst, F., Pereira, J.C.F., Schonung, B., 1983. Experimental and theoretical investigation of backward-facing step flow. *Journal of Fluid Mechanics*, 127, pp. 473–496.

[39] Abu-Mulaweh, H.I., 2003. Measurements of laminar mixed convection flow adjacent to an inclined surface with uniform wall heat flux. *International Journal of Thermal Sciences*, 42(1), pp. 57–62.